VELOCITY MEASUREMENTS IN A TURBULENT TRAILING VORTEX AND THEIR APPLICATION TO BWI NOISE PREDICTION

Semi-Annual Report to NASA Langley
under grant NAG-1-1119

by

William J Devenport,
Department of Aerospace and Ocean Engineering,
Virginia Polytechnic Institute and State University,
215 Randolph Hall, Blacksburg, VA 24061

and

Stewart A L Glegg,
Department of Ocean Engineering,
Florida Atlantic University,
Boca Raton, FL 33431

April 1991

Introduction

A two-year investigation of the trailing vortex shed by a rectangular NACA 0012 wing is in progress under the above grant. The objectives of this investigation are to observe the turbulence structure and spectral characteristics of this flow over a range of conditions and to incorporate these observations into the blade-wake interaction (BWI) noise-prediction method of Glegg(1989). This report is divided into four sections as follows:-

1. Measurements performed during the first year.
2. Presentation and discussion of a representative sample of the results.
3. Implications for the BWI noise prediction method.
4. Re-evaluation of work planned for the second year.

1. Measurements performed during the first year.

Experiments are being performed in the Virginia Tech Stability Wind Tunnel. So far the measurements have included helium-bubble flow visualizations and single-point hot-wire velocity measurements.

The visualizations, which are described in detail by Devenport and Sharma (1990), were taken over the range of Reynolds numbers and angles of attack listed in table 1. These showed the vortex to be relatively stable (moving less than ~5% chord across the tunnel) and insensitive to probe interference, making useful hot-wire velocity measurements possible.

The following velocity measurements have been made at conditions listed in table 2.

(a) Single hot-wire measurements at the wing trailing edge. These include detailed profiles and power spectra of the streamwise component of velocity. The purpose of these is to reveal the properties of the boundary layer shed from the wing.

(b) X-array hot-wire measurements in the vortex. Detailed profiles of all mean velocity and Reynolds stress components. Single-point spectra of all velocity components at representative radial positions.

(c) Triple hot-wire measurements in the vortex. Detailed profiles of all mean velocity and Reynolds stress components. Single-point spectra of all velocity components at representative radial positions. Long-time-record measurements at selected radial locations to deduce the statistical characteristics of the vortex motions.

2. Presentation and Discussion of Experimental Results.

Figure 1 shows the coordinate directions (X,Y,Z) (U,V,W) to be used in presenting results. The wing chord c, of 8", will be used to normalize distances. The nominal undisturbed free-stream velocity U_{ref} will be used to non-dimensionalize velocities. The thickness and state of the boundary-layer leaving the wing are listed in table 3 for each of the flow conditions.

Figures 2, 3 and 4 show velocity measurements made during a Z-wise traverse through the center of the vortex at X/c = 30, $Re_c = U_{ref}c/\nu$ = 400000, with the wing at 5° angle of attack (rotating from the X to the Z axis). Note that Z is measured relative to the center of the vortex.

In the vicinity of the vortex center (figure 2) the mean-velocity field is much as would be expected given the results of Mason and Marchman (1972). The tangential velocities associated with the vortex are clearly visible in the W component profile (figure 2(b)). These increase to a peak at the edge of the vortex core, which appears to have a diameter of about 0.72",(=0.09c). The small the core size is circumstantial evidence for the relative stability of the vortex and its insensitivity to probe interference. The U profile (figure 2(a)) shows an axial velocity deficit of about $0.12U_{ref}$. The normal stress profiles (figure 2(c)) are dominated in this region by a strong central peak. Here v^2/U_{ref}^2 and w^2/U_{ref}^2 reach peak values of 0.0064 (8% turbulence intensity) and u^2/U_{ref}^2 a peak of 0.0007 (2.6%). The large values of v^2 and w^2 are almost certainly due to a combination of the the small lateral motions of the vortex observed in the flow visualizations and the steep W gradient in the core. Approximate modeling of these motions, described in the appendix, show them to have an rms amplitude of less than 2mm. Observations of the velocity signals during the measurement suggest they have a frequency between about 1 and 10 Hz.

Away from the vortex center (figure 3) the results reveal a flow structure somewhat different from what we had expected. Here the measurements show two, if not three, distinct half turns of the wing wake as it spirals around the vortex. These appear as peaks in the normal and shear-stress profiles (figures 3(c) and (d)) and inflections and depressions the W and U profiles (figures 3(b) and (a)) respectively, centered at Z = +6", -2.5" and +1.5". In contrast to the results and discussion of previous workers (in particular Phillips and Graham (1984)) there appears to be little or no region surrounding the core in which the successive turns of the wing wake have merged to form a continuous axisymmetric structure. The behavior of the turbulence stresses in the spiral wake is especially

interesting. w^2 (the upwash component) is easily the largest stress, being typically 1.5 times u^2 and twice v^2. The magnitude of the normal stresses fall by about 40% on each half turn of the spiral. The shear stresses (figure 3(d)), of which uw is the largest drop, even more rapidly. This suggests that the greater circumferential shear experienced by the wing wake towards the vortex center inhibits the development or motions of large stress-producing turbulent eddies. In interpreting the finer details of the turbulence structure it is important to realize that there is no significant mean motion along the spiral towards the center of the vortex and that, after a few chord lengths of initial development just downstream of the wing, the tangential velocity field probably changes little in scale or structure with streamwise distance. In other words turbulence structure appearing at a particular radial position at X/c=30 presumably developed at that position under the action of an fairly constant mean velocity field.

Figure 4 shows autospectra of upwash velocity (w) measured different distances from the vortex center (at Z = -4", -2", -1", -0.7", -0.35" and 0") normalized on w^2. Note that the discrete peaks in these spectra at frequencies above 2kHz are a result of electrical noise. At Z = -4" and -2" (to either side of the 2nd half turn of the spiral wake, figure 3(c)) the spectra are almost identical despite the fact that the turbulence levels at these two points are quite different. These spectra have a broad peak centered at about 300Hz, corresponding to a streamwise lengthscale (assuming Taylor's hypothesis) of about 4", a distance approximately equal to the width of the wing wake at X/c = 30. The existence of such large structures seems improbable, however, when one considers the significant tangential-velocity gradient across the wake at this location (figure 3(b)). Moving in towards the vortex center the upwash spectrum changes rapidly. Most noticeable is a large increase in the energy at very low frequencies (presumably associated with the lateral motions of the vortex) and the development of a strong peak around 600Hz, yet to be explained.

Because of the possible importance of the spiral structure to BWI noise generation we have included normal stress profiles showing its behavior over a range of conditions in figure 5. The spiral widens with distance downstream of the wing and the turbulence levels within it fall (figures 5(a), (b) and (c)). As one would expect, increasing the angle of attack, and thus the vortex circulation (figures 5(c), (d) and (e)) has exactly the same qualitative qualitative effect as moving downstream. Changing the Reynolds number (figures 5(c), (f), (g) and (h)) has some effect on turbulence levels within the spiral wake but does not otherwise appear to influence the flow structure.

3.Implications for the BWI noise prediction method

The BWI noise prediction method was based on the measurements of Phillips and Graham(1984) which showed the turbulence intensity decaying monotonically from the center of the vortex. A simplified model was developed for the distribution of the turbulence and this gave a reasonable fit to the measured noise spectra, but spectral shape was incorrect. In this section the original BWI turbulent flow model will be compared with the current set of measurements and suggestions made as to how this model could be improved.

For the flow conditions at a Reynolds number of 400000 the original BWI model predicts the distribution of normal turbulent stress shown in figure 6. This identifies some important departures from the measured levels given in figures 2(c) and 3(c). First note that the peak turbulent stress is predicted as 2.6×10^{-4} in comparison with the measured peak level of 64×10^{-4}. The large measured levels in the vortex core have been attributed to the lateral motion of the vortex whereas the BWI prediction scheme assumes purely turbulent motion relative to a fixed vortex. The significance of the large measured velocity fluctuations is questionable since it is argued that the lateral motions of the vortex do not cause BWI noise for the following reasons. First the velocity fluctuations only occur close to the core which is unlikely to be split by the blade. Secondly the vortex core is symmetric and so there will be equal upwash and downwash on the blade at any instant, causing an inefficient mechanism for producing an unsteady load. Thirdly the frequency spectra of the lateral vortex motions show more energy at low frequencies than would be expected from BWI noise measurements. We conclude therefore that, although the measured turbulence levels are highest close to the center of the vortex due to lateral motions, these are not significant for BWI noise.

Better insight is obtained by comparing figure 6 with figure 3(c) which is an expanded plot of figure 2(c). The measured and predicted turbulence levels, outside of the central core, are of the same magnitude although their distributions are quite different. It is clear that the original BWI prediction method uses an inadequate model of the turbulence structure and further consideration must be given to modelling this more accurately.

In the previous section the spiral structure of the flow about the vortex core was discussed. If we assume a flow with vorticity concentrated in the vortex core, which is not completely accurate for this flow, then a simple model of the spiral can be developed which enables some conclusions to be drawn about BWI noise generation. The azimuthal velocity outside the vortex core can be described as

$$V_\theta(r) = C\frac{v_0 r_0}{r} \qquad (1)$$

where C=1.398, and v_o is the peak azimuthal velocity which occurs at r_o (see appendix). Using equation (1) the azimuthal displacement of a particle, which is convected with a velocity U in the streamwise direction and a velocity V_θ in the azimuthal direction, is easily shown to be

$$\theta = C\frac{v_0 r_0 x}{Ur^2} \qquad (2)$$

where x is the downstream convection distance. The wake shed by the blade will be rolled up by this vortical motion, and a simplified wake model can be obtained using a wake with a constant initial width which is displaced according to equation (2). Calculations based on this approach lead to the wakes illustrated in figure 7 which shows how a downstream blade intersects a rolled up wake. It is clear from figure 7 that when the displacement of the blade from the center of the vortex is small, then the dominant feature of the flow is the vortex core and the inner part of the spiral. It has already been argued that the vortex core does not produce BWI noise, and so the inner part of the spiral is the most important region of turbulent flow. Figure 7 shows that when the blade is above the vortex (negative 'z') the spanwise length immersed in the spiral is small. Further the spiral is close to the core where the turbulence is significantly reduced. On the other hand when the blade is below the vortex (positive 'z') the blade is immersed in a significant length of turbulent wake, where the turbulence levels are highest. It would appear that this is the most important region for BWI noise production. However to predict the noise correctly it is necessary to know how the turbulence intensity is distributed in this part of the wake, what are the turbulence lengthscales as a function of frequency and what are the turbulence spectra.

It is also interesting to compare the original BWI model of the turbulence spectra with the measured spectra in the outer part of the spiral. These are given in figure 4 for two different locations and show very close similarity, suggesting that the spectra may be a universal function of the flow. The original prediction scheme assumed that the turbulence was isotropic with a Von Karman energy spectrum and an integral lengthscale defined as

$$L=0.672\,\gamma\,\Theta\,(x/\Theta+380)^{1/2}$$

where γ is an empirical constant, chosen as γ=0.8, and Θ is the momentum thickness of the wake. The upwash spectrum is then calculated as

$$G_{ww}(f) = \frac{\overline{w}^2 L}{\pi U}\left\{\frac{1+(14/3)\hat{k}_1^2}{(1+\hat{k}_1^2)^{11/6}}\right\}$$

where

$$\hat{k}_1 = \frac{\omega L}{1.34U}$$

Spectra based on this model are shown in figure 8 and clearly indicate more low frequency energy and a slower decay at high frequencies than measured in the wake spiral. These features were also found in the predicted BWI noise spectrum when they were compared with measured noise levels. This suggests that if the turbulence spectra measured here were used for noise predictions better results would be obtained.

4. Re-evaluation of Work Planned for the Second Year.

The BWI noise prediction model needs to be updated to incorporate a suitable model of the flow in the wake spiral. This will require:

-models for the spiral wake boundaries, and the turbulence stress distributions,
-models of the spectral distribution and lengthscales of the turbulence.

To develop these models further measurements are clearly needed. Specifically,

-detailed measurements of turbulence stress distributions throughout the spiral,
-measurements showing the variation of velocity spectra along and across the spiral,
-measurements of lengthscales along and across the spiral at a number of different positions within the spiral.

In addition to providing quantitive input for the BWI noise prediction method, these data are needed to obtain a clear physical understanding of the flow. Such an understanding is essential if the models to be developed for the noise prediction method are to have any generality. With this in mind we beleive it will be most effective to concentrate on obtaining a detailed and complete data set at one flow condition (say X/c=30, Re_c=400000, 5° angle of attack). It should be possible to infer the

effects of streamwise distance, Reynolds number and angle of attack from the measurements already made.

5. References

Devenport W.J. and Sharma G., 1990, "Flow visualizations of a wing-tip vortex in the presence of a probe", VPI&SU, Report VPI-AOE-177, September.

Glegg S.A.L., 1989, "The prediction of blade-wake interaction noise based on a turbulent vortex model", AIAA 89-1134, presented at the 12th Aeroacoustics Conference, San Antonio, Texas.

Howe M.S., 1988, "Research on Lifting Surface Noise", BBN Report 6890, Bolt Beranek and Newman, Cambridge, Mass.

Mason W H and Marchman J F, 1972, "Farfield structure of an aircraft trailing vortex, including effects of mass injection", NASA CR 62078.

Phillips W R C and Graham J A H, 1984, "Reynolds stress measurements in a turbulent trailing vortex", Journal of Fluid Mechanics, vol 147, p 353.

Schlinker R.H. and Amiet R. K.,(1983), "Rotor-Vortex Interaction Noise", AIAA 83-0720, Presented at the 8th AIAA Aeroacoustics Conference, Atlanta, Georgia

Appendix: Simulation of Lateral Vortex Motions

The flow visualizations showed small lateral perturbations of the vortex by the tunnel flow. Since there are large velocity gradients in the velocity field of the vortex, the perturbations will induce additional unsteady velocity fluctuations at a fixed measurement point. The purpose of this appendix is to evaluate this effect using a simplified model of the mean velocity profile in the vortex.

The Mean Velocity Profile of the Vortex

Schlinker and Amiet (1983) and Howe (1988) define a model of the azimuthal and axial velocity in a vortex as a function of the radial distance from it's center. This model couples a solid body rotation in the viscous core with a 1/r decay in the outer region. The azimuthal velocity is given by:

$$V_\theta(r) = C\frac{v_0 r_0}{r}\left[1 - e^{-\alpha(r/r_0)^2}\right] \qquad \text{(A1)}$$

where α=1.25643 and C=(1+0.5/α)= 1.398. The maximum azimuthal velocity is v_o and occurs at a radius of r_o. The circulation is given by $\Gamma_o = 2\pi(1+\alpha/2)v_o r_o$.

The axial velocity deficit model is

$$U(r) = U_{ref} - U_D e^{-\alpha(r/r_0)^2} \qquad \text{(A2)}$$

where U_D is the axial velocity deficit on the centerline.

The experimental results suggest that $v_o = 0.24U_{ref}$, r_o=0.36" and $U_D = 0.12U_{ref}$. Using these parameters the predicted mean velocity profiles are given in Figures A1 and A2. In general this model gives a good fit to the azimuthal velocity in the viscous core but underpredicts the velocity in the outer region, suggesting that the field is not decaying as rapidly as expected from the simple model given here. The width of the axial velocity deficit is also underpredicted. However, in this analysis we are concerned with the velocity induced by lateral motions of the vortex core which will not be affected by errors in the outer region or in the axial velocity deficit.

The Unsteady Velocity Components

Consider the vortex center as displaced from the center of the co-ordinate system by **z** which is a random function of observer time at a fixed streamwise location (see figure 3). A turbulent eddy located at **x** relative to the origin of the co-ordinate system, is displaced from the center of the vortex by **y**, such that $\mathbf{x}=\mathbf{y}+\mathbf{z}(t)$. The mean velocity field of the vortex is defined as $\mathbf{V}(\mathbf{y})$ and the unsteady turbulence component is $\mathbf{v}(\mathbf{y},t)$ and are a function of the displacement from the vortex center. The velocity measured by a fixed probe will have a mean component $\mathbf{U}(\mathbf{x})$ and an unsteady component $\mathbf{u}(\mathbf{x},t)$, given by

$$\mathbf{U}(\mathbf{x})+\mathbf{u}(\mathbf{x},t)=\mathbf{V}(\mathbf{x}-\mathbf{z}(t))+\mathbf{v}(\mathbf{x}-\mathbf{z}(t),t)$$

If the displacements of the vortex are small in comparison with the the core radius then we can expand the right hand side of this equation in a Taylor series, to first order,

$$\mathbf{U}(\mathbf{x})+\mathbf{u}(\mathbf{x},t)=\mathbf{V}(\mathbf{x})+\mathbf{v}(\mathbf{x},t)-(\mathbf{z}(t).\nabla)(\mathbf{V}+\mathbf{v})$$

This shows that the measured mean component $\mathbf{U}(\mathbf{x})$ is, to first order, the same as the mean flow about the vortex. The unsteady component is a combination of the turbulence associated with the vortex and velocity fluctuations induced by the time varying lateral displacements.

We assume that **v** and $\mathbf{z}=(0,\alpha,\beta)$ are uncorrelated so that the mean square velocity components are

$$\left\langle \mathbf{u}^2 \right\rangle = \left\langle \mathbf{v}^2 \right\rangle + \left\langle \left(\alpha \frac{\partial \mathbf{V}}{\partial y} + \beta \frac{\partial \mathbf{V}}{\partial z} \right)^2 \right\rangle \qquad \text{(A3)}$$

If the vortex displacements can be assumed to be isotropic with an rms displacement ε, so that

$$\langle \alpha^2 \rangle = \langle \beta^2 \rangle = \varepsilon^2 \quad \text{and} \quad \langle \alpha\beta \rangle = 0 \qquad \text{(A4)}$$

the three components of the normal turbulent stresses due to the lateral vortex motion can be defined as

$$\left\langle u'^2 \right\rangle = \varepsilon^2 \left\{ \left(\frac{\partial U}{\partial y} \right)^2 + \left(\frac{\partial U}{\partial z} \right)^2 \right\}$$

$$\left\langle v'^2 \right\rangle = \varepsilon^2 \left\{ \left(\frac{\partial V}{\partial y} \right)^2 + \left(\frac{\partial V}{\partial z} \right)^2 \right\}$$

$$\left\langle w'^2 \right\rangle = \varepsilon^2 \left\{ \left(\frac{\partial W}{\partial y} \right)^2 + \left(\frac{\partial W}{\partial z} \right)^2 \right\}$$

where **V**=(U,V,W). By using the mean velocity profiles described in the previous section we obtain

$$V = -\frac{z}{r} V_\theta(r) \qquad W = \frac{y}{r} V_\theta(r)$$

so that

$$\frac{\partial U}{\partial y} = \frac{y}{r} \frac{\partial U}{\partial r} \qquad \frac{\partial U}{\partial z} = \frac{z}{r} \frac{\partial U}{\partial r} \tag{A5}$$

$$\frac{\partial V}{\partial y} = -\frac{zy}{r^2} \left\{ r \frac{\partial}{\partial r} \left(\frac{V_\theta}{r} \right) \right\} \qquad \frac{\partial V}{\partial z} = -\frac{V_\theta}{r} - \frac{z^2}{r^2} \left\{ r \frac{\partial}{\partial r} \left(\frac{V_\theta}{r} \right) \right\} \tag{A6}$$

$$\frac{\partial W}{\partial y} = \frac{V_\theta}{r} + \frac{y^2}{r^2} \left\{ r \frac{\partial}{\partial r} \left(\frac{V_\theta}{r} \right) \right\} \qquad \frac{\partial W}{\partial z} = \frac{zy}{r^2} \left\{ r \frac{\partial}{\partial r} \left(\frac{V_\theta}{r} \right) \right\} \tag{A7}$$

The measurements were taken on y=0 and so these equations can be simplified to give the three components of the normal turbulent stresses as

$$\left\langle u'^2 \right\rangle = \varepsilon^2 \left(\frac{\partial U}{\partial r} \right)^2$$

$$\left\langle v'^2 \right\rangle = \varepsilon^2 \left(\frac{V_\theta}{r} + r \frac{\partial}{\partial r} \left(\frac{V_\theta}{r} \right) \right)^2 = \varepsilon^2 \left(\frac{\partial V_\theta}{\partial r} \right)^2$$

$$\left\langle w'^2 \right\rangle = \varepsilon^2 \left(\frac{V_\theta}{r} \right)^2$$

By using equations A1 and A2 we obtain

$$\left\langle u'^2 \right\rangle = \varepsilon^2 \left(U_D \frac{2\alpha r}{r_0^2} e^{-\alpha(r/r_0)^2} \right)^2 \qquad \text{(A8)}$$

$$\left\langle v'^2 \right\rangle = \varepsilon^2 \left(C \frac{v_0 r_0}{r^2} \left[1 - \left(1 + 2\alpha (r/r_0)^2 \right) e^{-\alpha(r/r_0)^2} \right] \right)^2 \qquad \text{(A9)}$$

$$\left\langle w'^2 \right\rangle = \varepsilon^2 \left(C \frac{v_0 r_0}{r^2} \left[1 - e^{-\alpha(r/r_0)^2} \right] \right)^2 \qquad \text{(A10)}$$

Notice here that as 'r' becomes small we can approximate

$$1\text{-}\exp(-\alpha(r/r_0)2) \approx \alpha(r/r_0)2$$

so that

$$\left\langle w'^2 \right\rangle = \left\langle v'^2 \right\rangle = \varepsilon^2 \left(C \frac{\alpha v_0}{r_0} \right)^2 = 3.08 \left(\frac{\varepsilon v_0}{r_0} \right)^2$$

In figure 2(c) we see that $\langle v'^2 \rangle = \langle w'^2 \rangle = 0.0064 U_{ref}^2$ and since $v_o = 0.24 U_{ref}$ and $r_o = 0.36$", we can compute ε as 0.0683"(1.73mm).

Figure A4 shows the predicted normal turbulent stresses obtained using this model and the agreement with the measurements in Figure 2(c) is excellent. The only noticeable error is in the predicted value of $\langle u'^2 \rangle$ close to z=0. However the effects of finite probe size and low turbulence levels at this point may cause he predicted dip to be filled in.

The turbulent shear stresses can also be predicted using this approach, since

$$\langle u'v' \rangle = \varepsilon^2 \left\{ \left(\frac{\partial U}{\partial y} \right) \left(\frac{\partial V}{\partial y} \right) + \left(\frac{\partial U}{\partial z} \right) \left(\frac{\partial V}{\partial z} \right) \right\}$$

$$\langle u'w' \rangle = \varepsilon^2 \left\{ \left(\frac{\partial U}{\partial y} \right) \left(\frac{\partial W}{\partial y} \right) + \left(\frac{\partial U}{\partial z} \right) \left(\frac{\partial W}{\partial z} \right) \right\}$$

$$\langle v'w' \rangle = \varepsilon^2 \left\{ \left(\frac{\partial V}{\partial y} \right) \left(\frac{\partial W}{\partial y} \right) + \left(\frac{\partial V}{\partial z} \right) \left(\frac{\partial W}{\partial z} \right) \right\}$$

Inspection of equations A5,A6, and A7 shows that the only non-zero turbulent shear stress on y=0 is the <u'v'> component which is given by

$$\langle u'v' \rangle = \varepsilon^2 \left\{ \left(\frac{\partial U}{\partial z} \right) \left(\frac{\partial V}{\partial z} \right) \right\} = \varepsilon^2 \left\{ \left(\frac{\partial U}{\partial r} \right) \left(\frac{\partial V_\theta}{\partial r} \right) \right\}$$

In terms of the simplified model this can be defined as

$$\langle u'v' \rangle = \varepsilon^2 \left(U_D \frac{2\alpha r}{r_0^2} e^{-\alpha (r/r_0)^2} \right) \left(C \frac{v_0 r_0}{r^2} \left[1 - \left(1 + 2\alpha (r/r_0)^2 \right) e^{-\alpha (r/r_0)^2} \right] \right)$$

and is plotted in figure A5. Comparing figure A5 with figure 2(d) shows that there is a significant discrepancy between the predicted and measured levels. First the predicted values if <uv> are much higher than measured and secondly the measured values of the <wv> shear stress is not negligible. These features of the flow do not appear to be explained by this simplified model

Reynolds number	Angle of attack
1.3×10^5	2.5°
	5°
	7.5°
2.6×10^5	5°
	7.5°
4.0×10^5	2.5°
	5°
	7.5°
5.3×10^5	5°

Table 1. Flow conditions for helium bubble visualizations (120 grade sandpaper trip).

Reynolds no.	Angle of attack	Axial pos z/c	Boundary layer trip
1.3×10^5	5°	30	Glass beads
2.6×10^5	5°	30	Glass beads
4.0×10^5	0°	30	Glass beads
	2.5°	30	Glass beads
	5°	30	Glass beads
	5°	25	Glass beads
	5°	20	Glass beads
	7.5°	30	Glass beads
5.3×10^5	5°	30	Glass beads
	5°	30°	None

Table 2. Flow conditions and locations of hot-wire measurements.

Angle of attack (degrees)	Side	Reynolds number Re_c	Thickness[1] (inches)	State
0	S	400000	0.353	Turb.
	P		0.357	Turb.
2.5	S	400000	0.390	Turb.
	P		0.323	Turb.
5.0	S	130000	0.420	Trans.
	P		0.270	Trans.
	S	260000	0.413	Turb.
	P		0.300	Low Re Turb.
	S	400000	0.418	Turb.
	P		0.292	Turb.
	S	530000	0.437	Turb.
	P		0.298	Turb.
7.5	S	400000	0.552	Turb.
	P		0.270	Turb

Table 3. Boundary-layer thickness and state at the wing trailing edge with the glass-beads trip. (S) - suction side, (P) - pressure side. State infered from mean-velocity and turbulence intensity profiles.

[1]Defining the boundary layer edge as the point of 2% turbulence intensity.

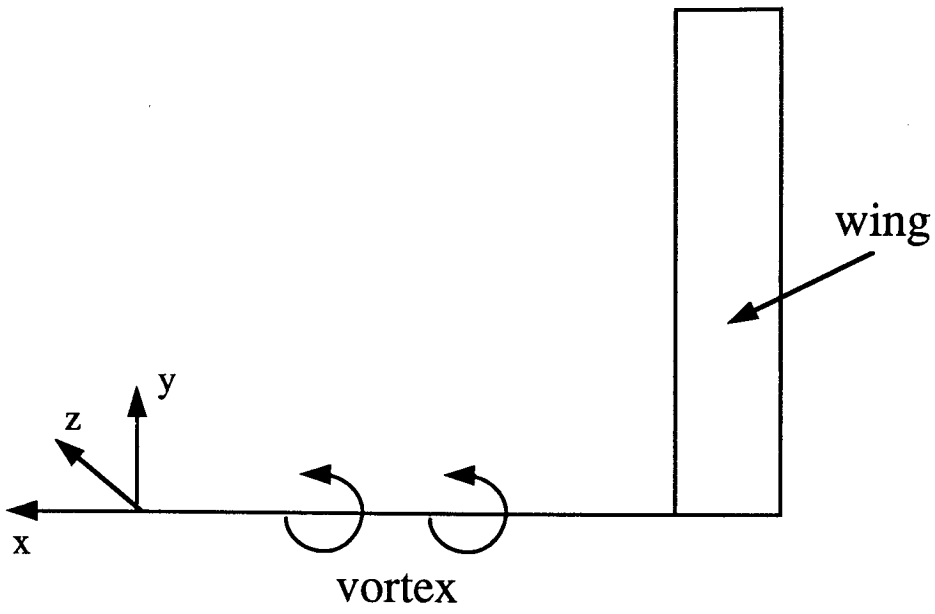

Figure 1: The co-ordinate system for the trailing tip vortex

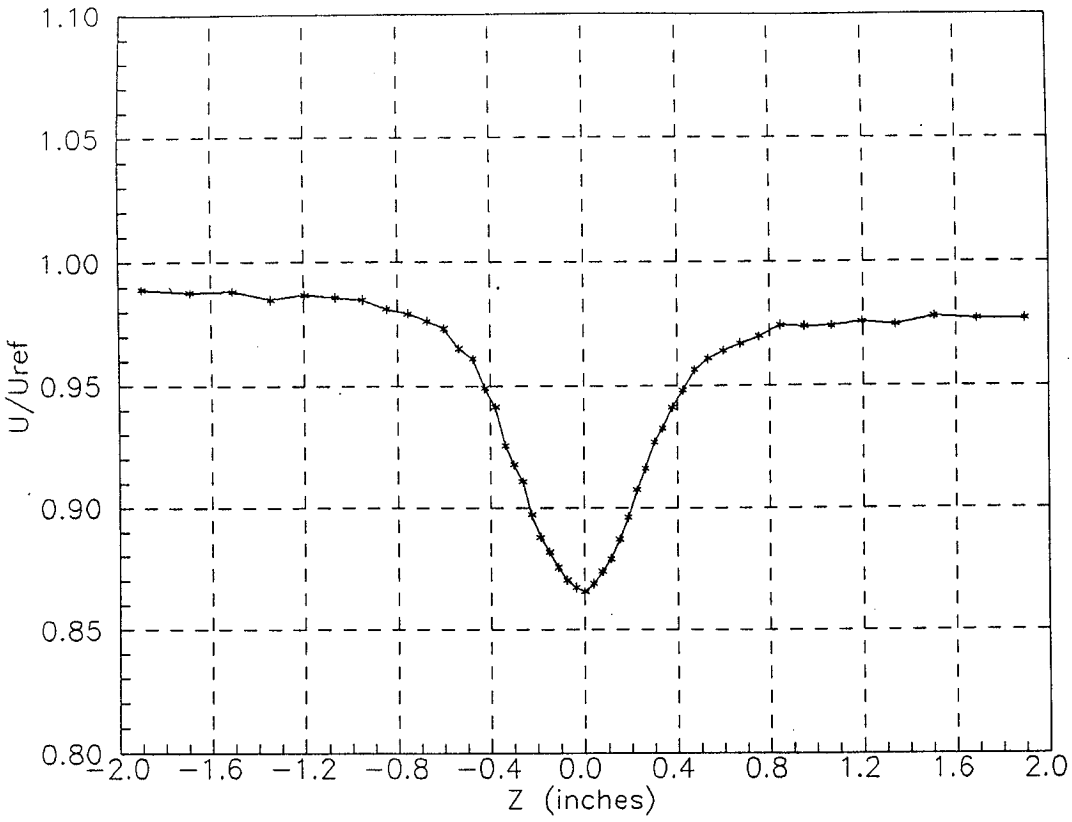

(a) Profile of U/U_{ref}.

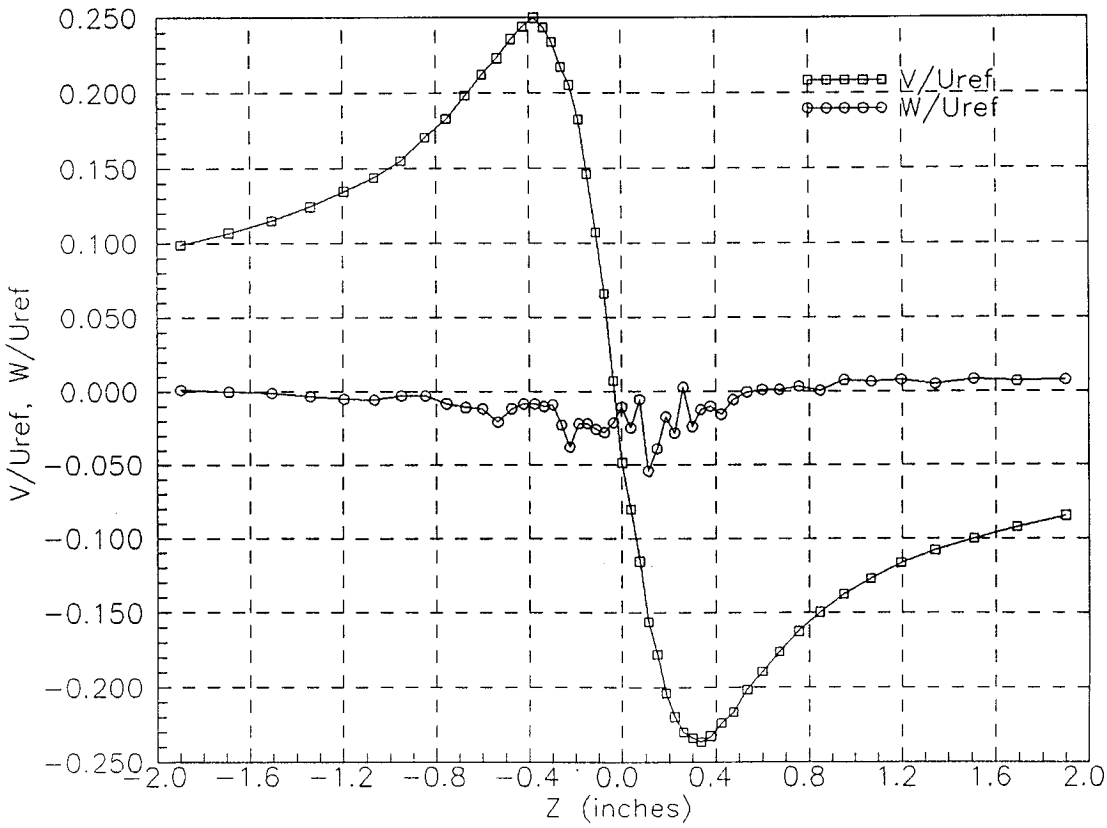

(b) Profiles of V/U_{ref} and W/U_{ref}.

Figure 2. Velocity measurements near the vortex center at $X/c = 30$, $Re_c = 400000$, 5° angle of attack.

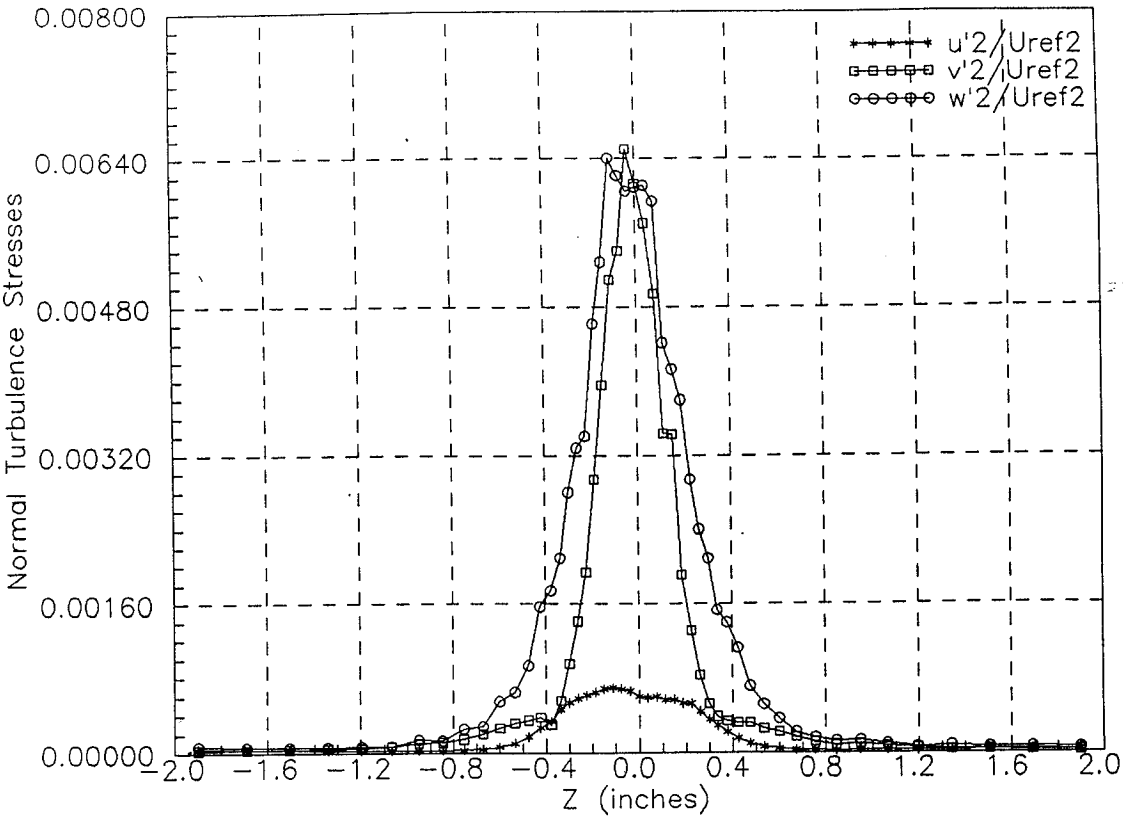

(c) Profiles of the normal turbulence stresses.

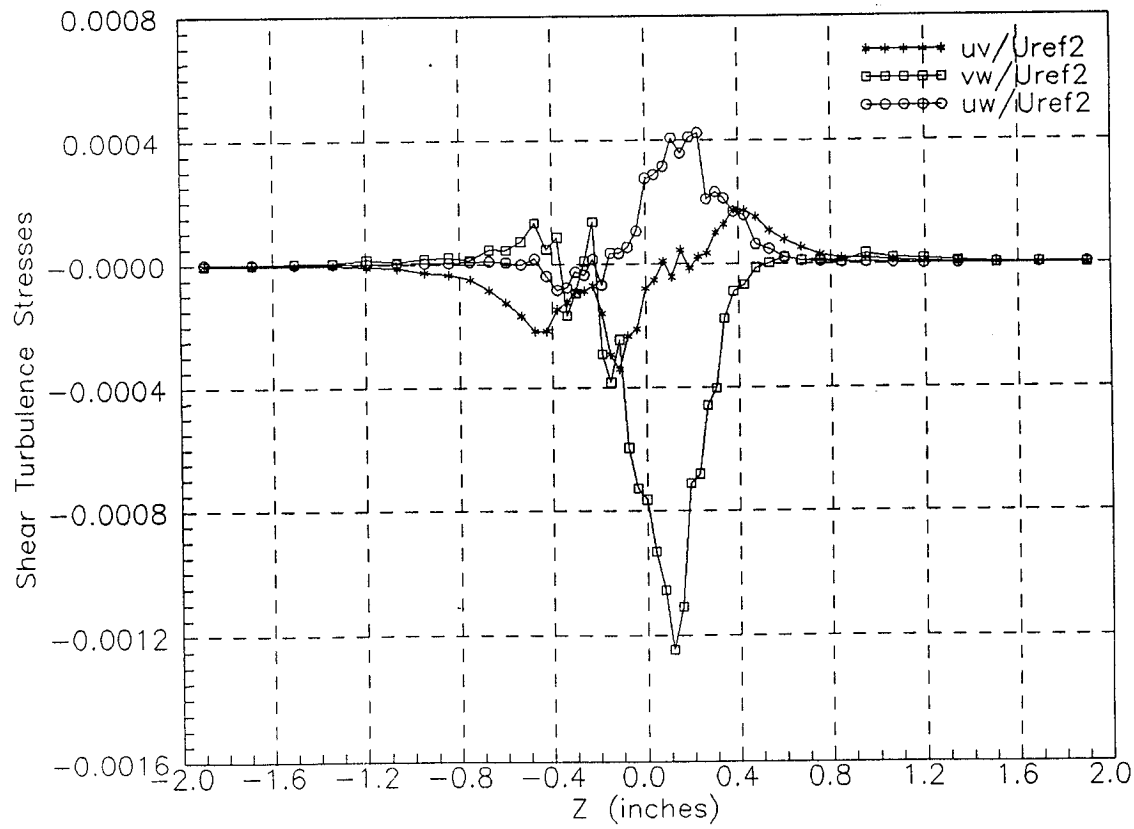

(d) Profiles of the turbulence shear stresses.

Figure 2. Velocity measurements near the vortex center at X/c = 30, Re_c = 400000, 5° angle of attack.

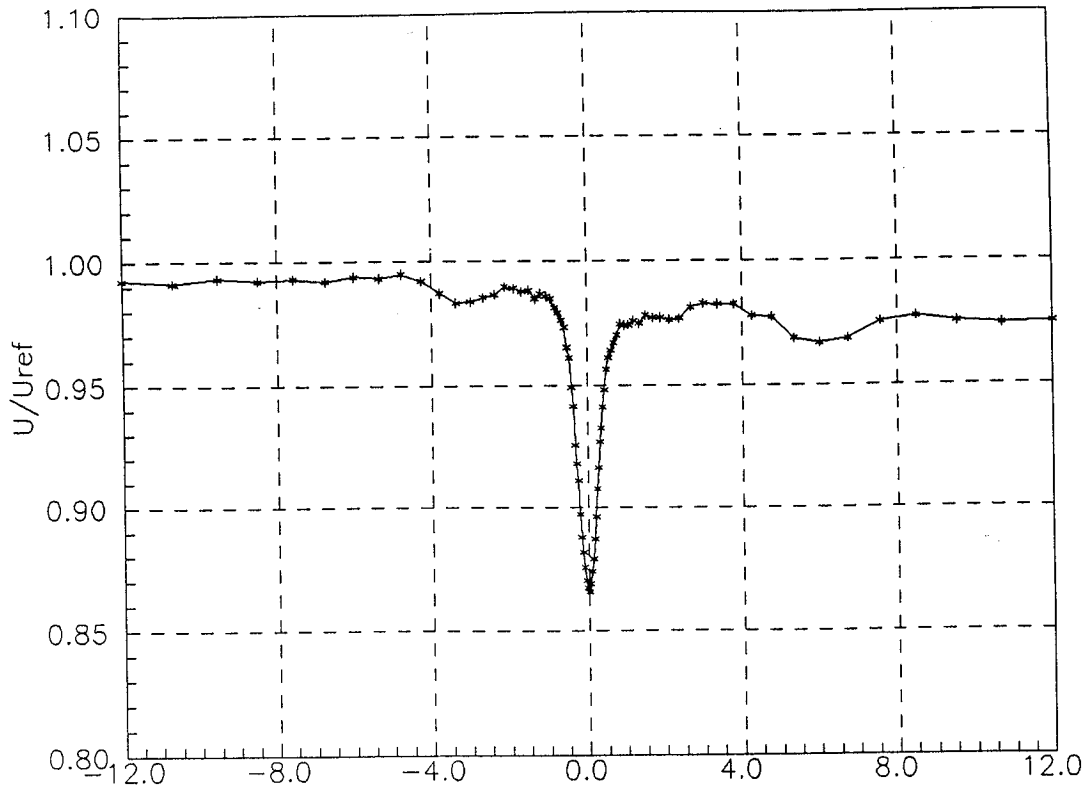

(a) Profile of U/U_{ref}.

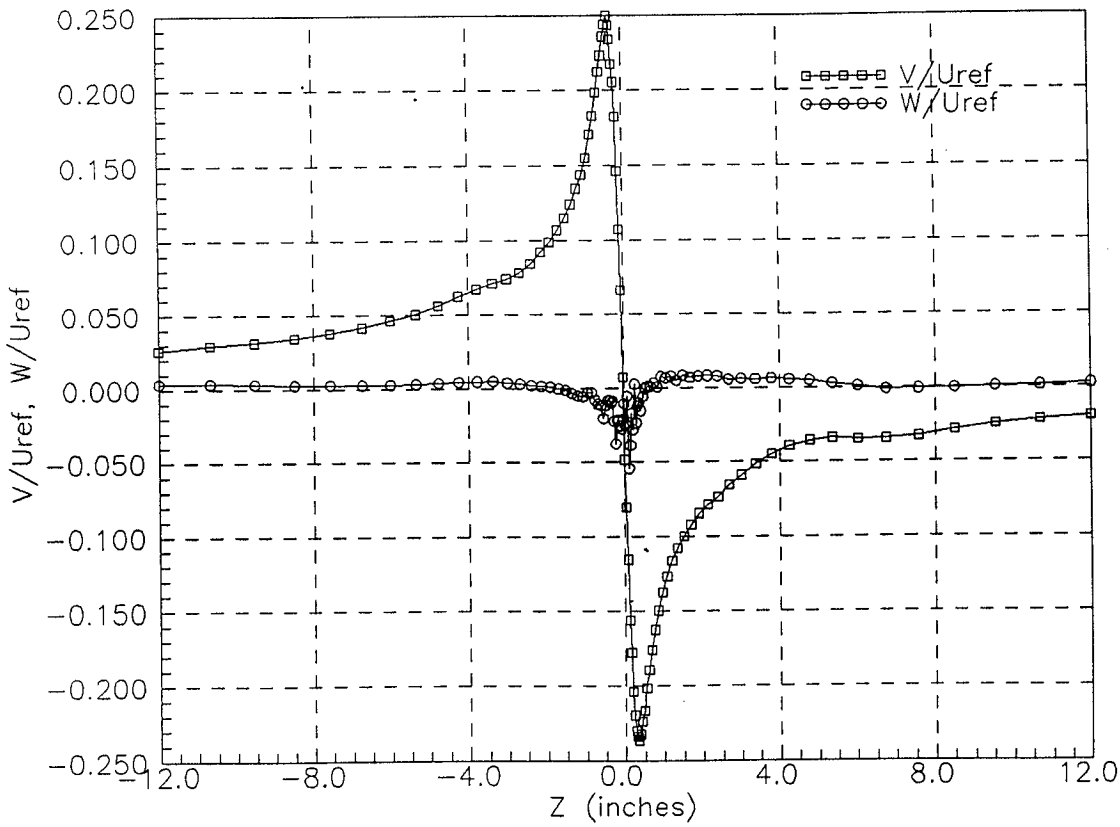

(b) Profiles of V/U_{ref} and W/U_{ref}.

Figure 3. Velocity measurements away from the vortex center at X/c = 30, Re_c = 400000, 5° angle of attack.

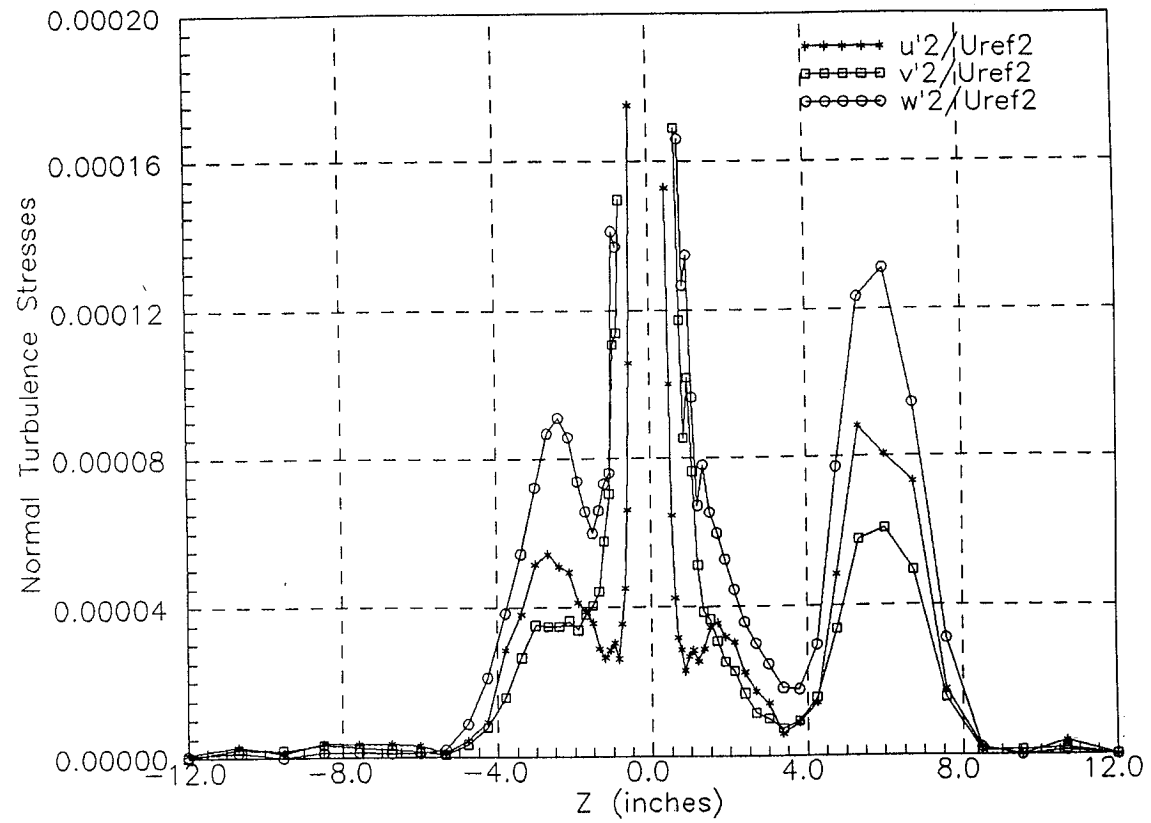

(c) Profiles of the normal turbulence stresses.

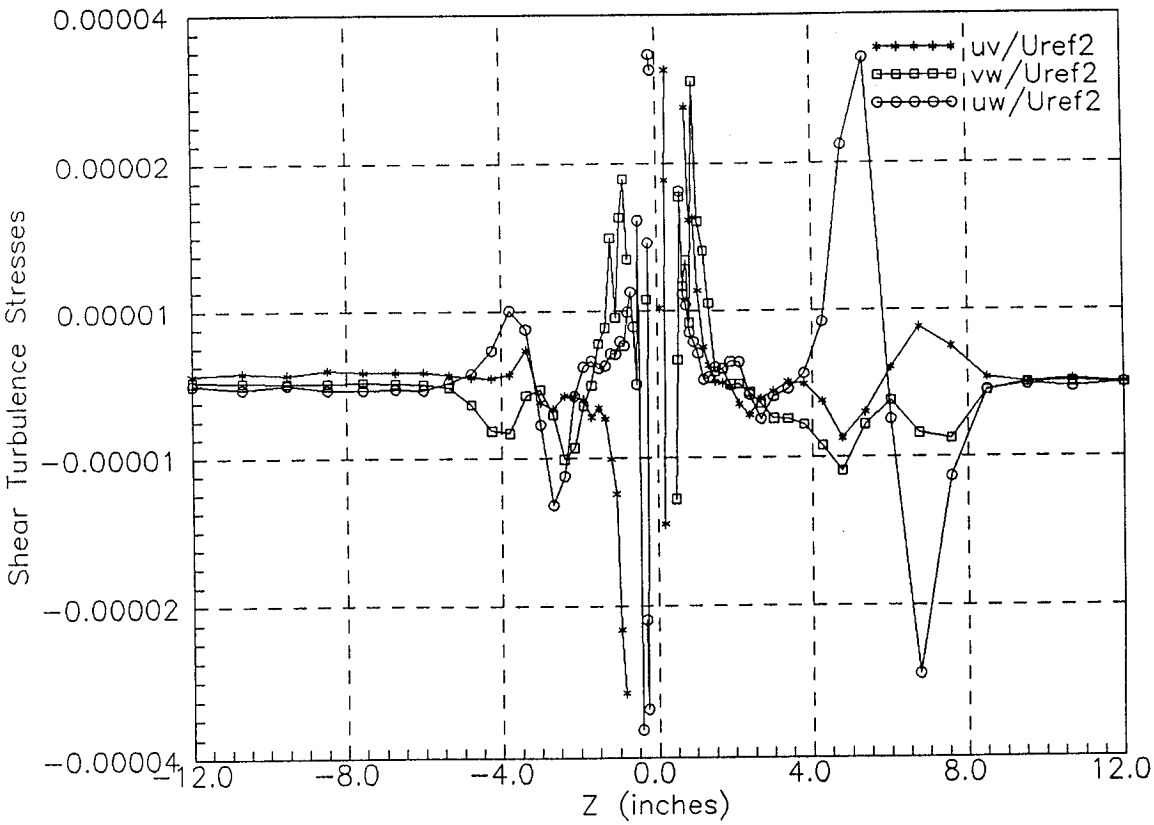

(d) Profiles of the turbulence shear stresses.

Figure 3. Velocity measurements away from the vortex center at X/c = 30, Re_c = 400000, 5° angle of attack.

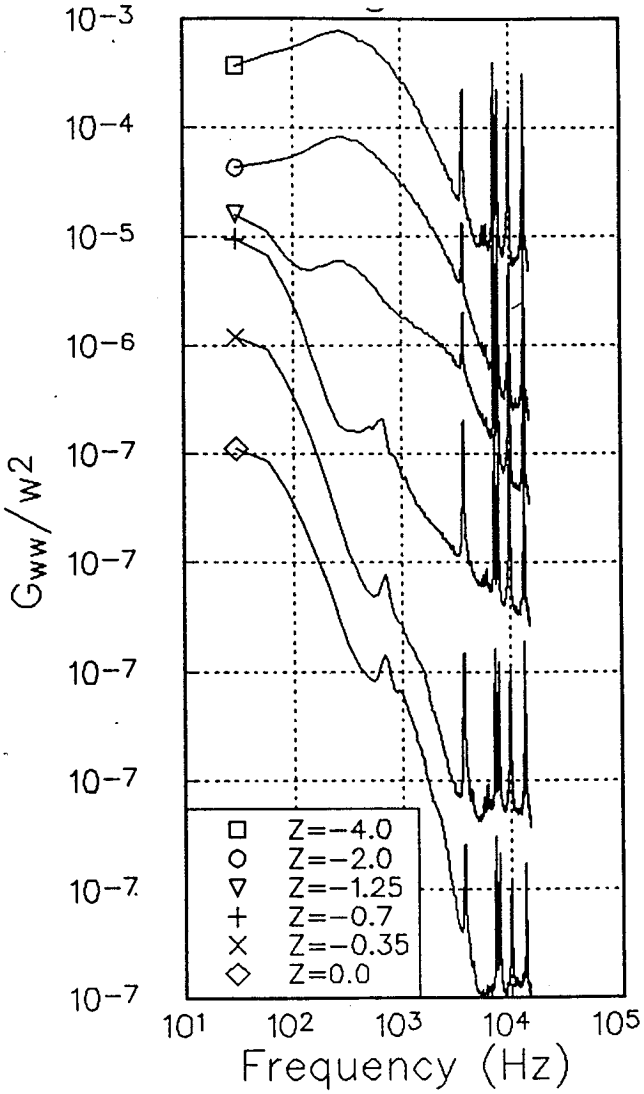

Figure 4. Power spectra of upwash velocity fluctuations measured at X/c = 30, Re = 400000, 5° angle of attack.

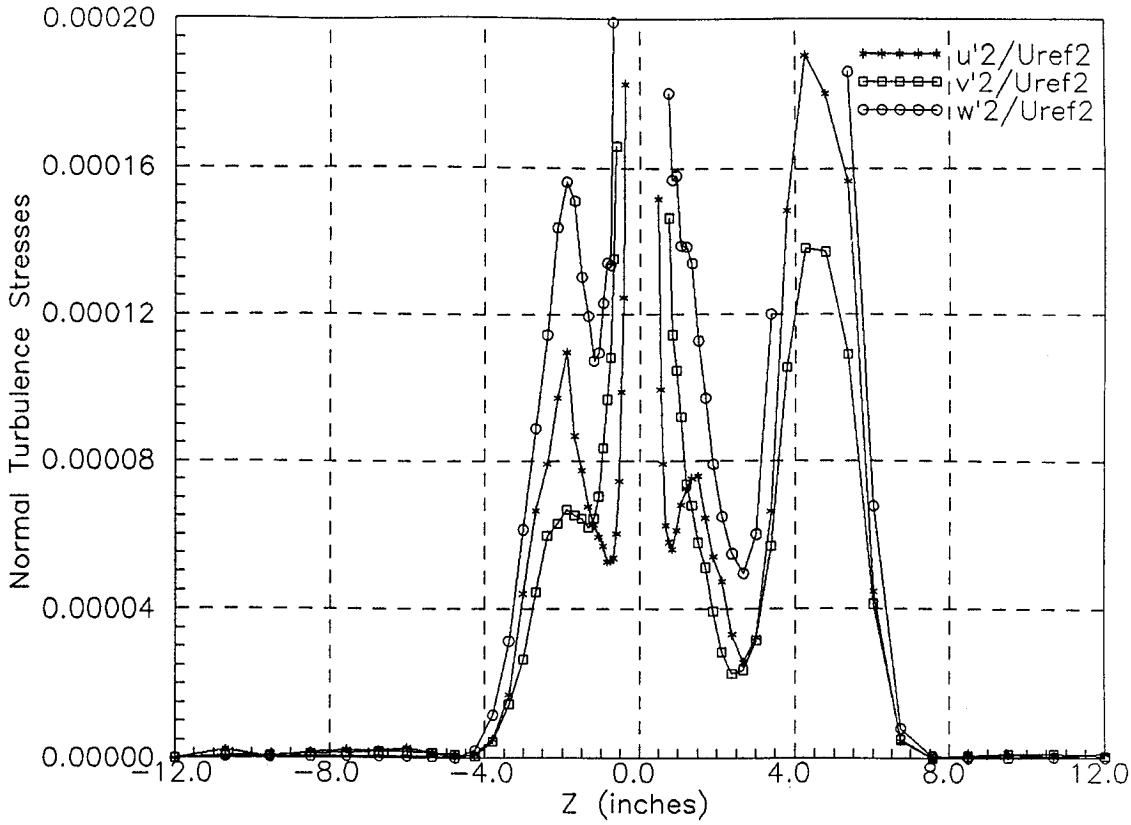

(a) X/c = 20, Re_c = 400000, 5° angle of attack.

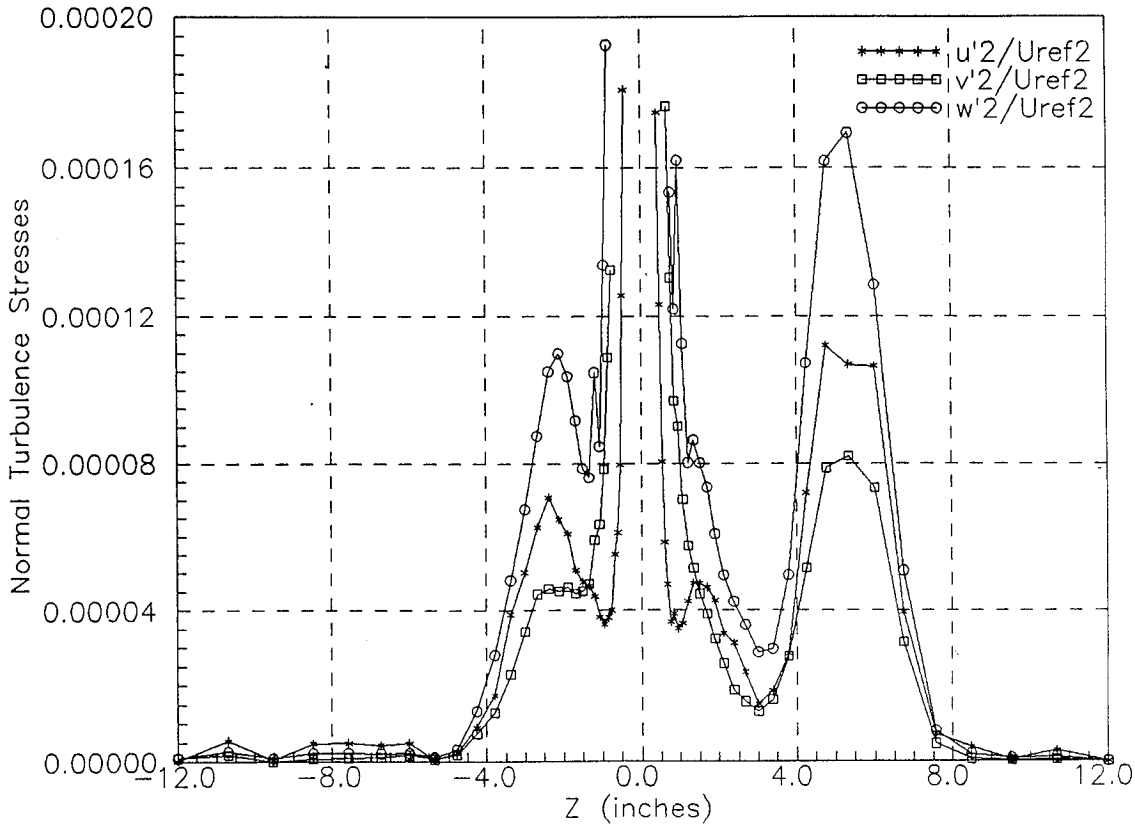

(b) X/c = 25, Re_c = 400000, 5° angle of attack.

Figure 5. Normal turbulence stress profiles measured away from the vortex center.

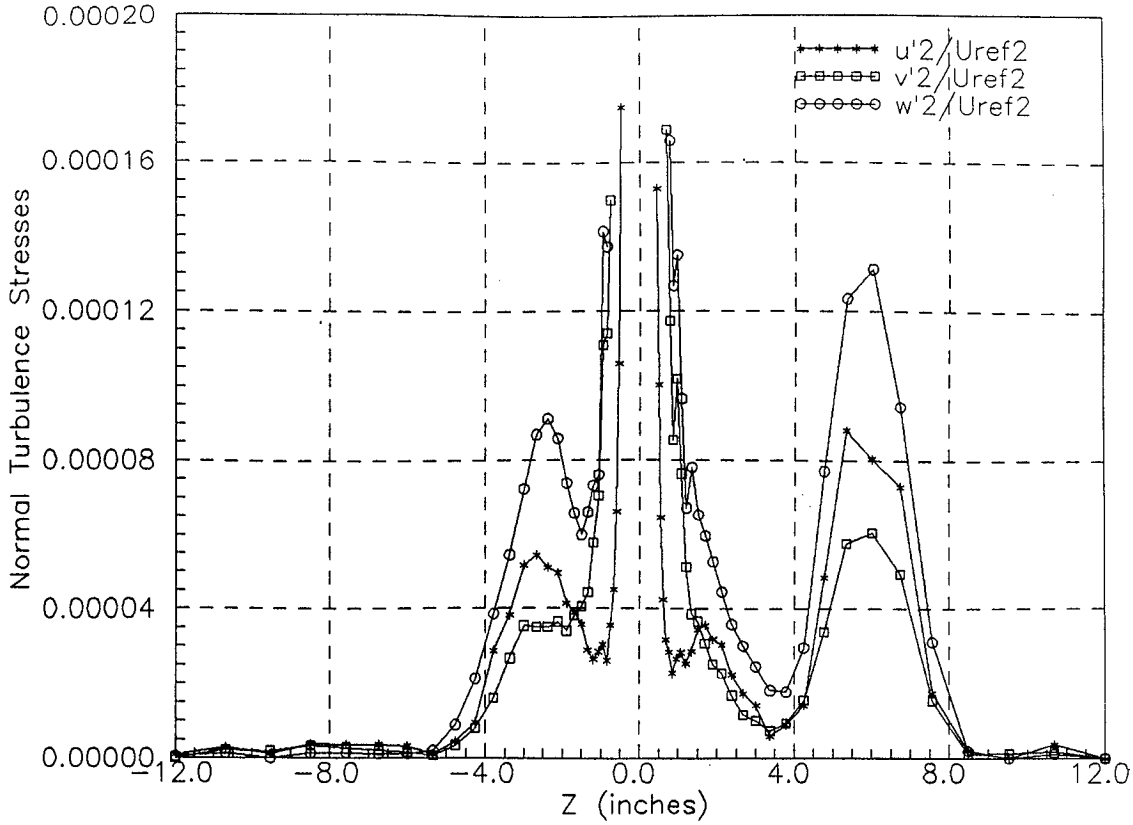

(c) X/c = 30, Re_c = 400000, 5° angle of attack.

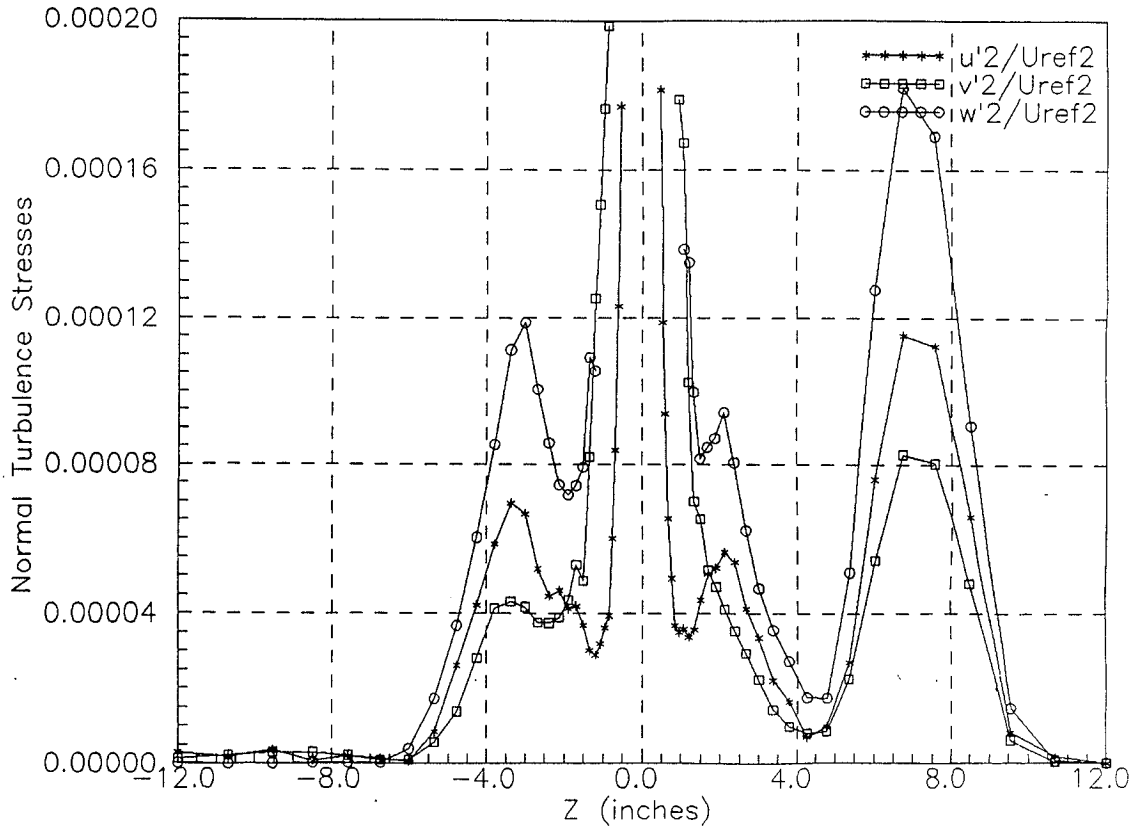

(d) X/c = 30, Re_c = 400000, 7.5° angle of attack.

Figure 5. Normal turbulence stress profiles measured away from the vortex center.

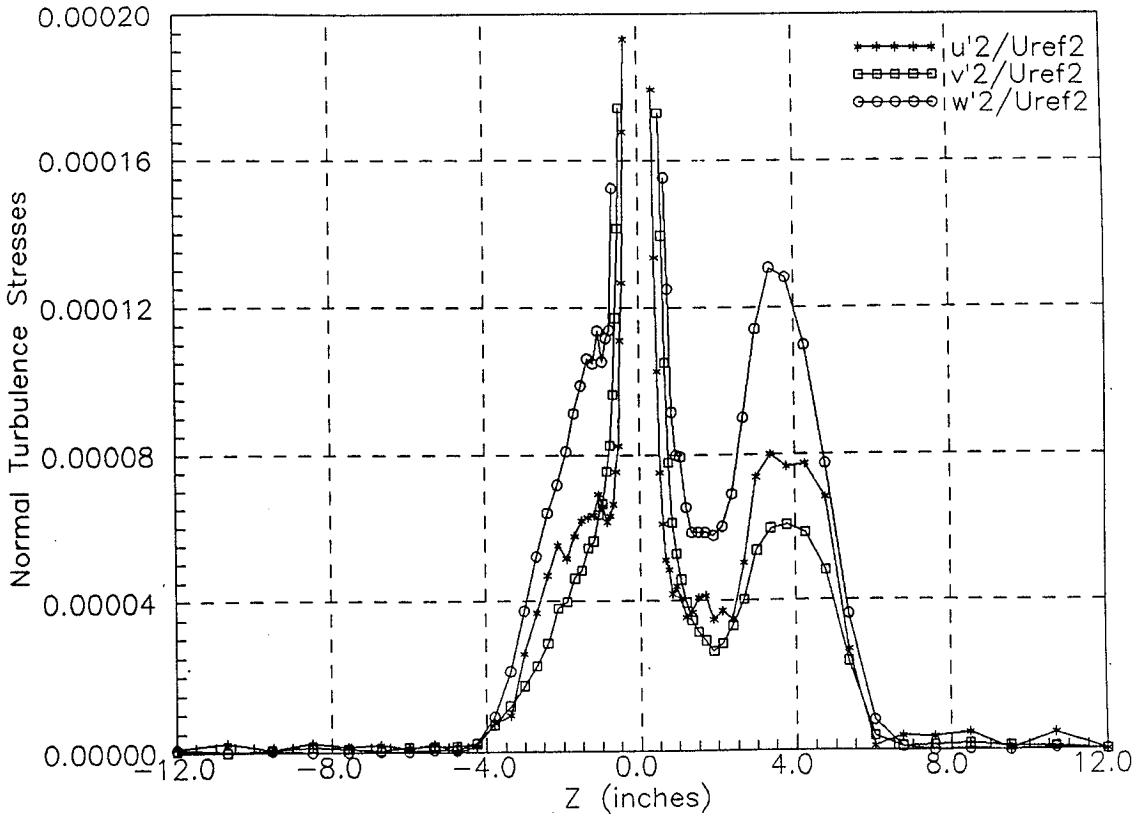

(e) X/c = 30, Re_c = 400000, 2.5° angle of attack.

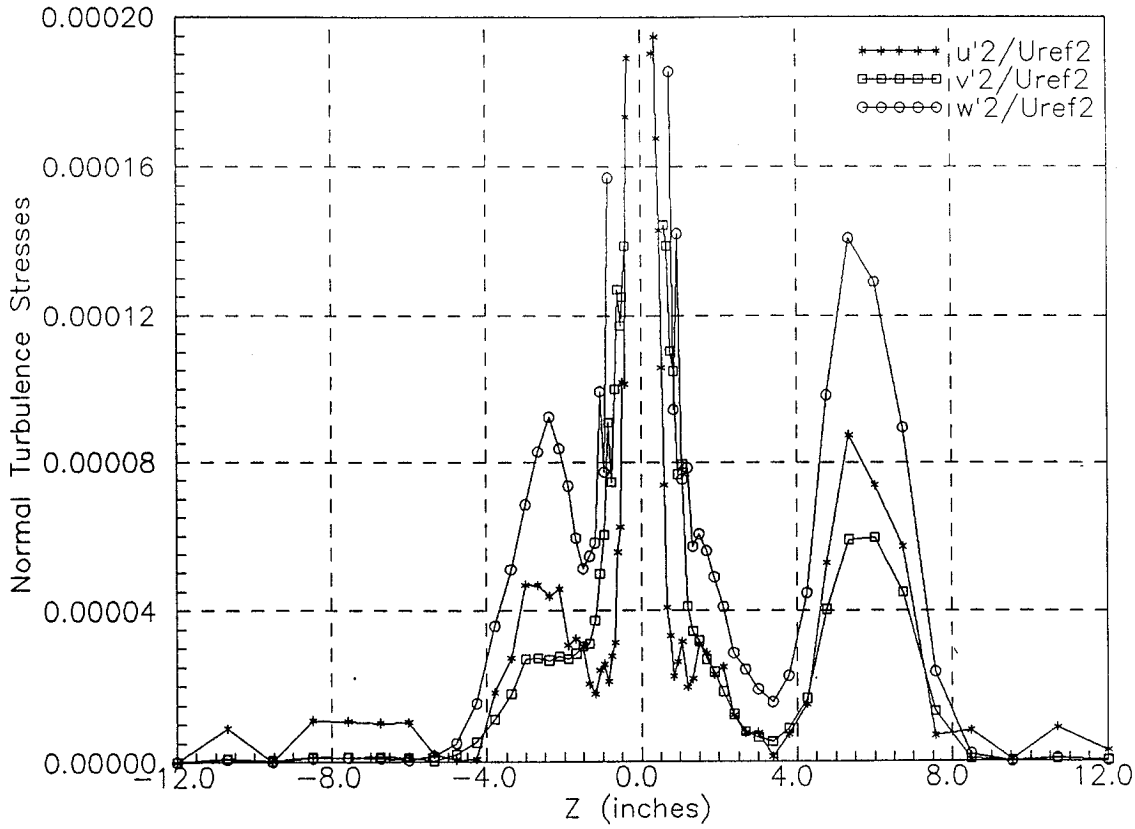

(f) X/c = 30, Re_c = 130000, 5° angle of attack.

Figure 5. Normal turbulence stress profiles measured away from the vortex center.

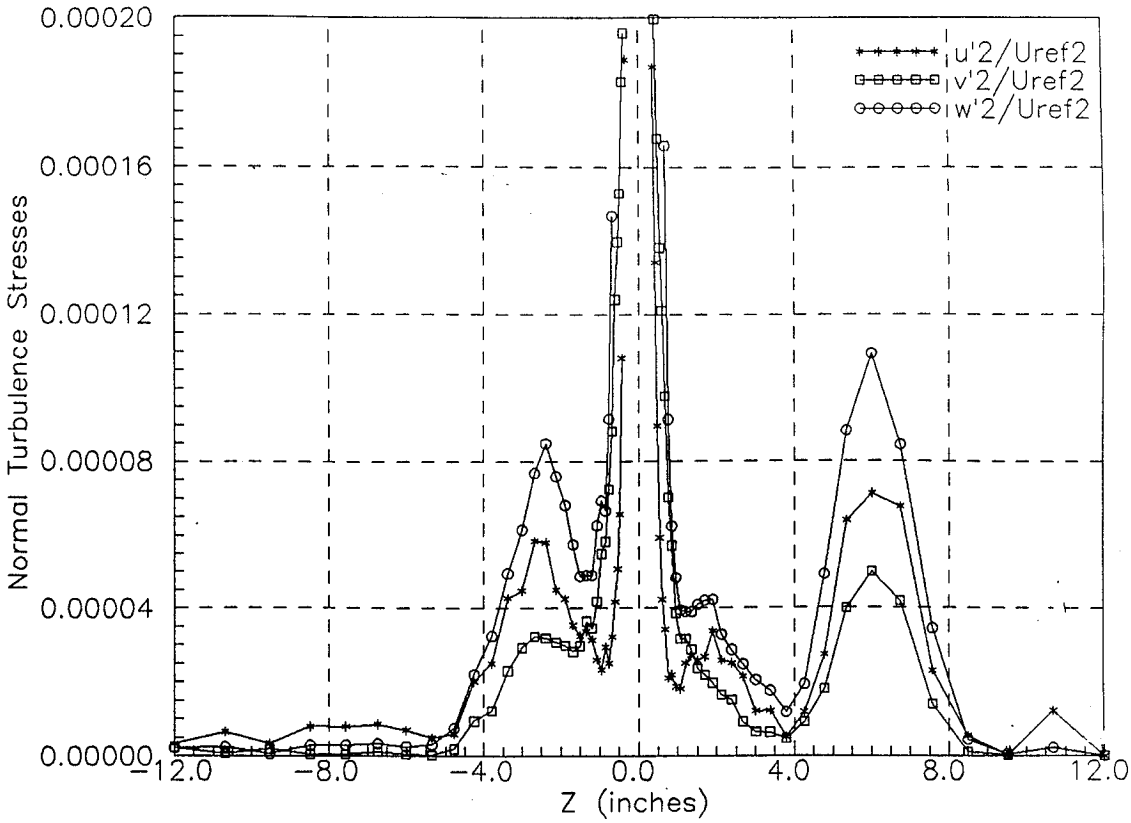

(g) X/c = 30, Re_c = 260000, 5° angle of attack.

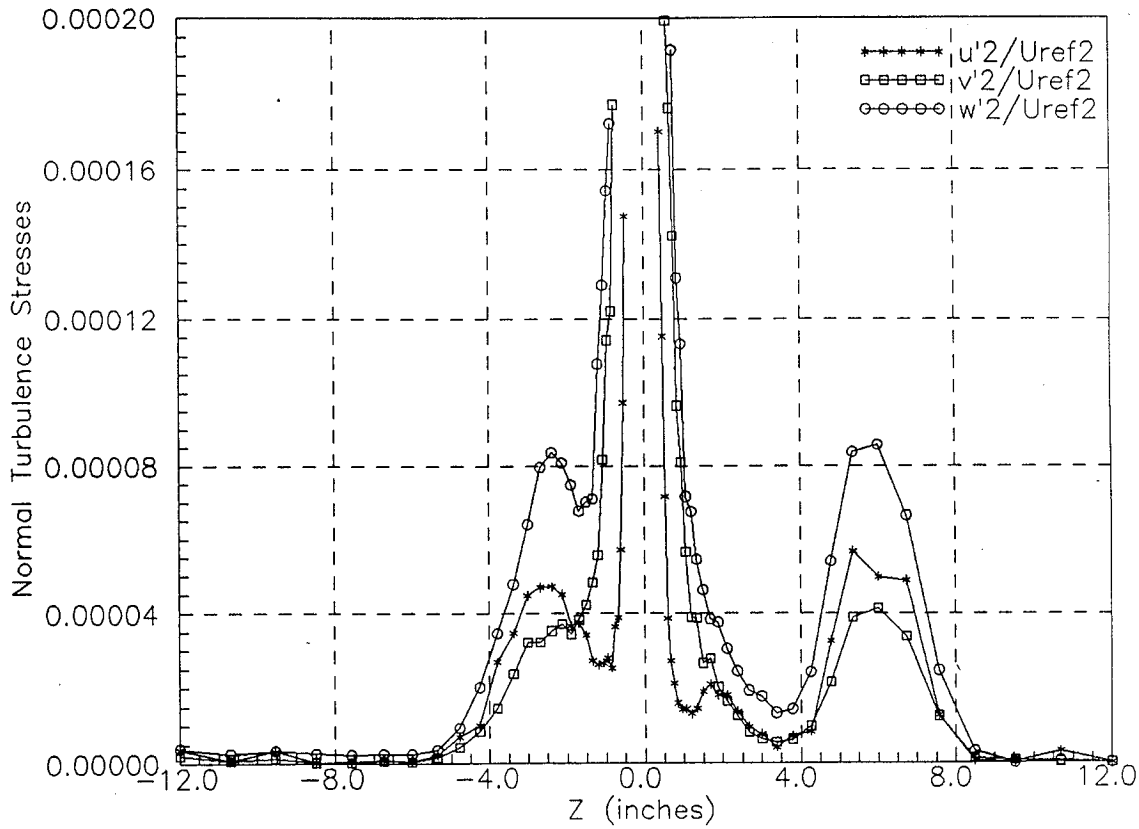

(h) X/c = 30, Re_c = 530000, 5° angle of attack.

Figure 5. Normal turbulence stress profiles measured away from the vortex center.

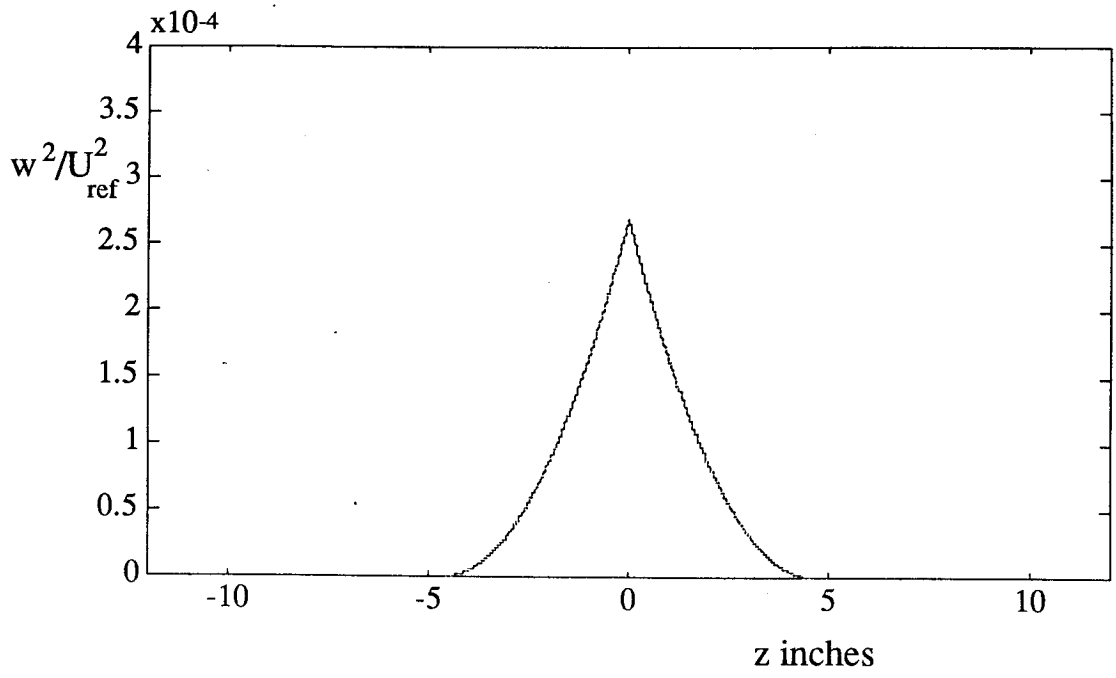

Figure 6: Predicted normal turbulent stress using the original BWI model

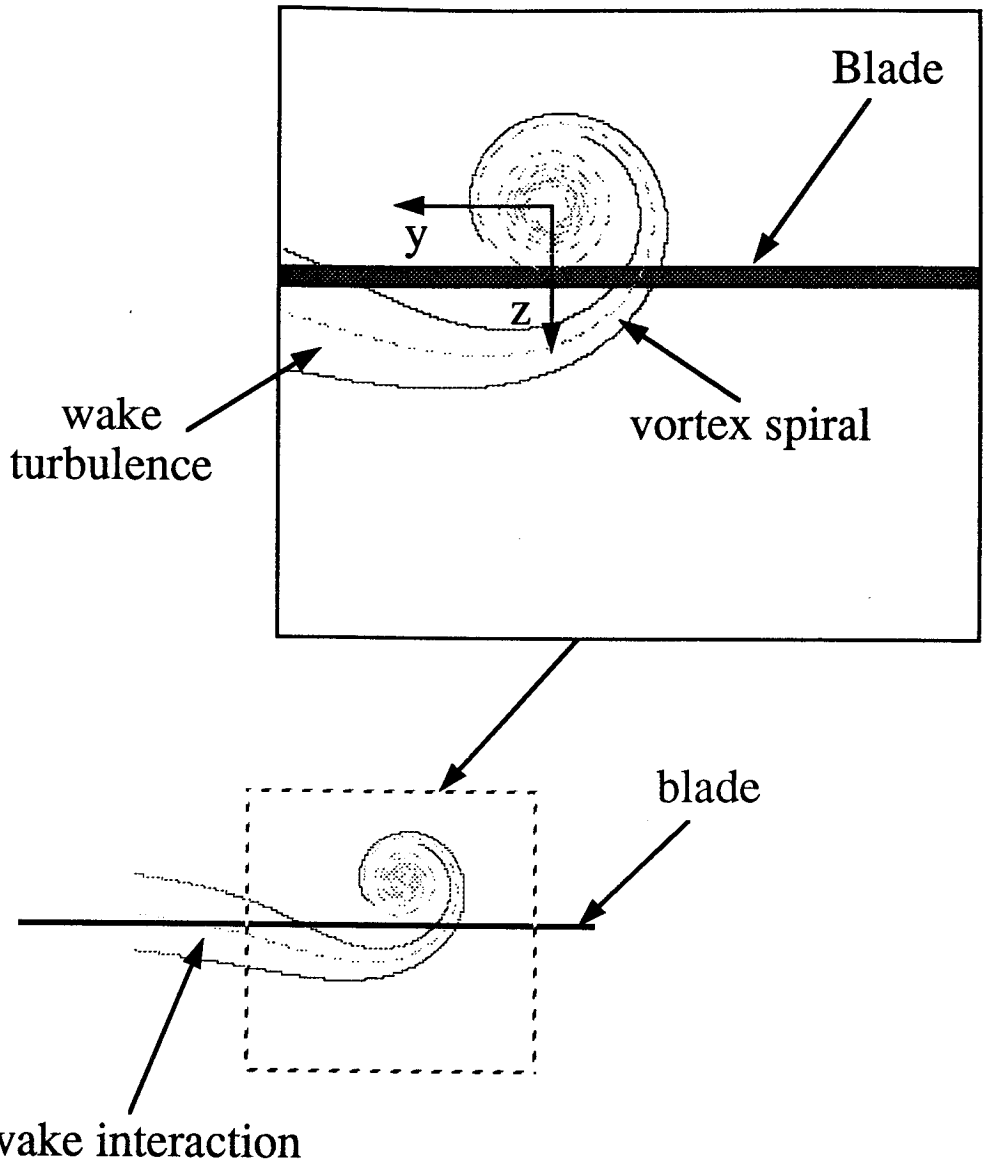

Figure 7:The vortex spiral interacting with a rotor blade

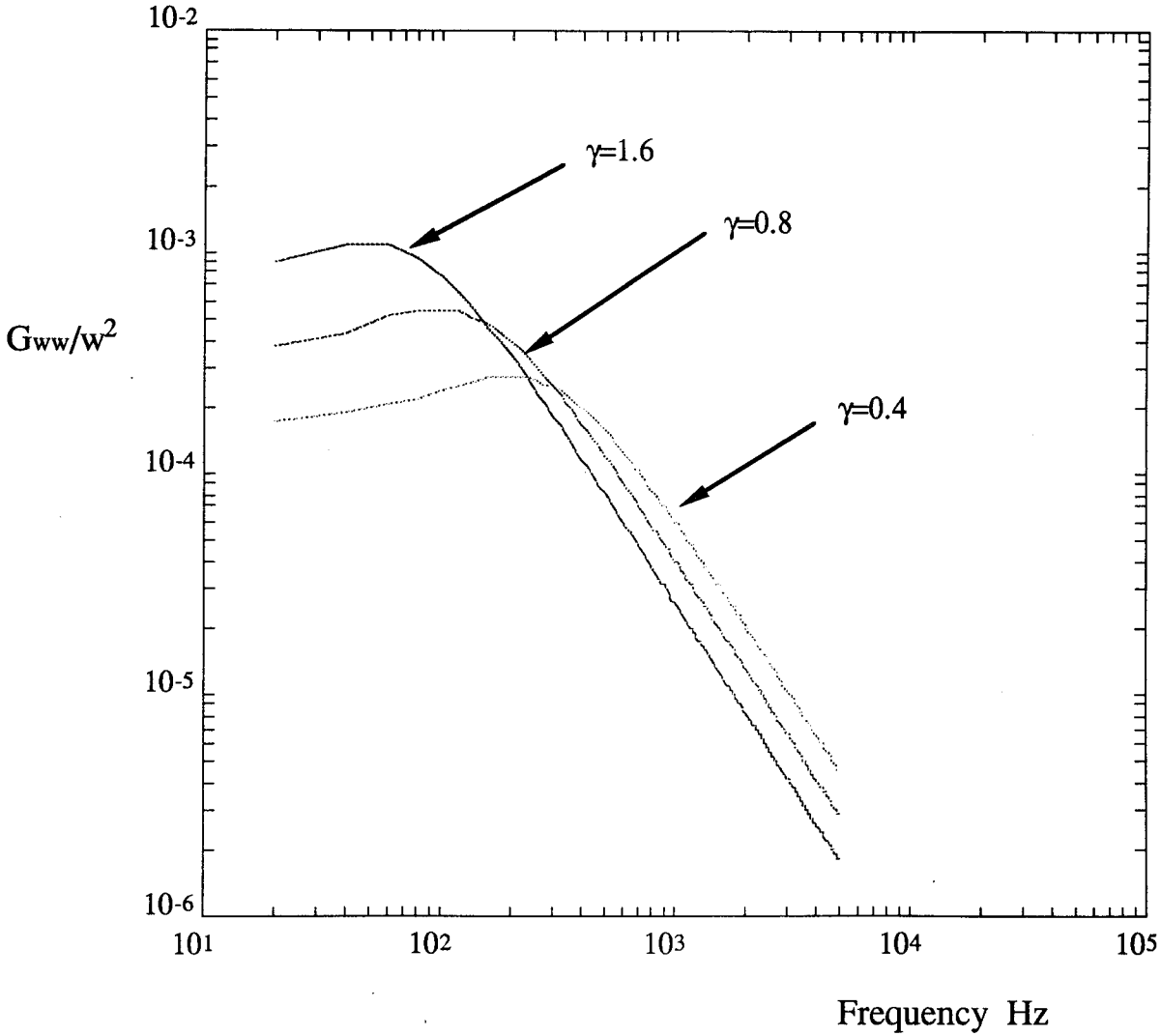

Figure 8: G_{ww}/w^2 verses frequency using the parameters and model of the original BWI program with γ =0.4,0.8,1.6

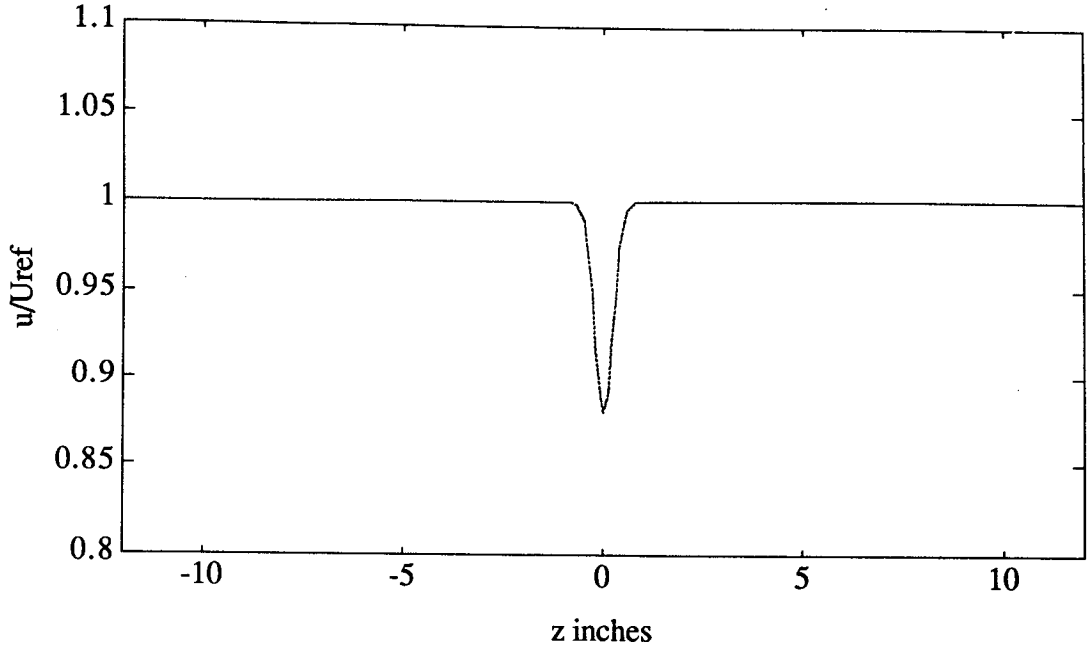

Figure A1: The axial velocity profile predicted using equation A2 with $U_D=0.12U_{ref}$ and $r_o=0.36"$

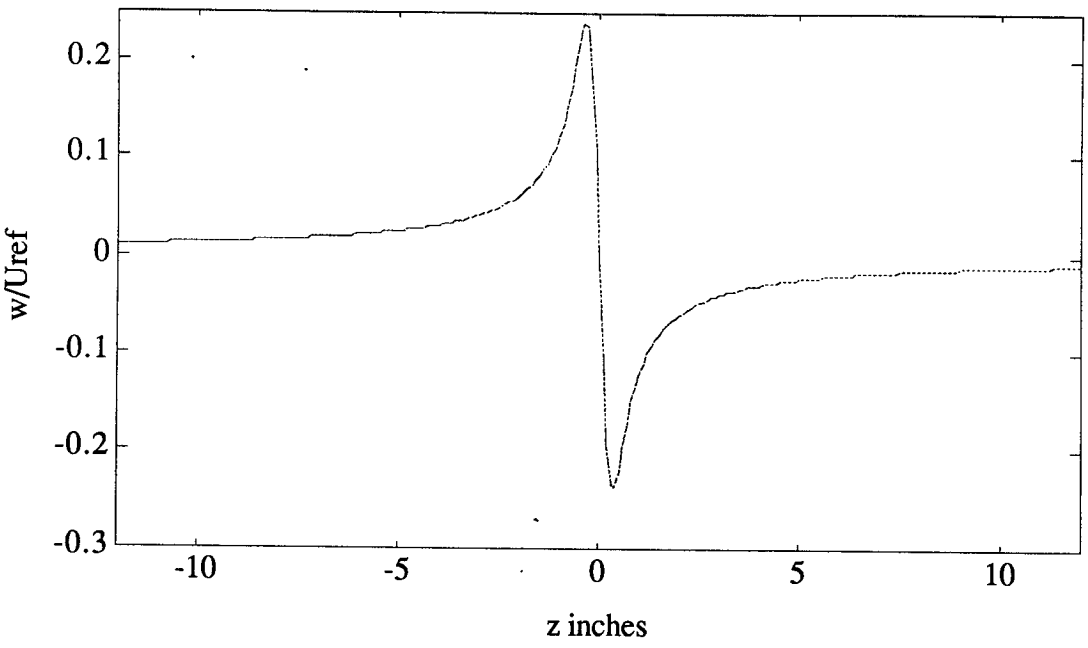

Figure A2: The azimuthal velocity profile predicted using equation A1 with $v_o=0.24U_{ref}$ and $r_o=0.36"$

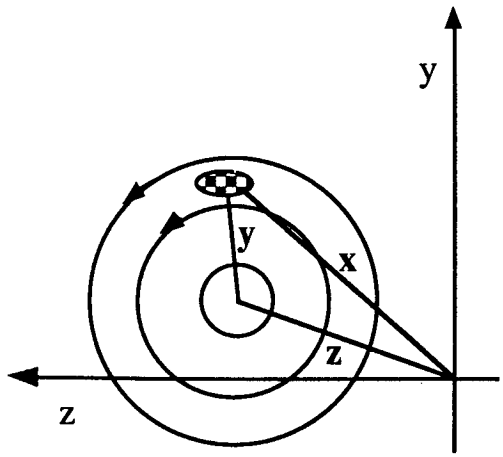

Figure A3: The co-ordinate system relative to the center of the vortex.

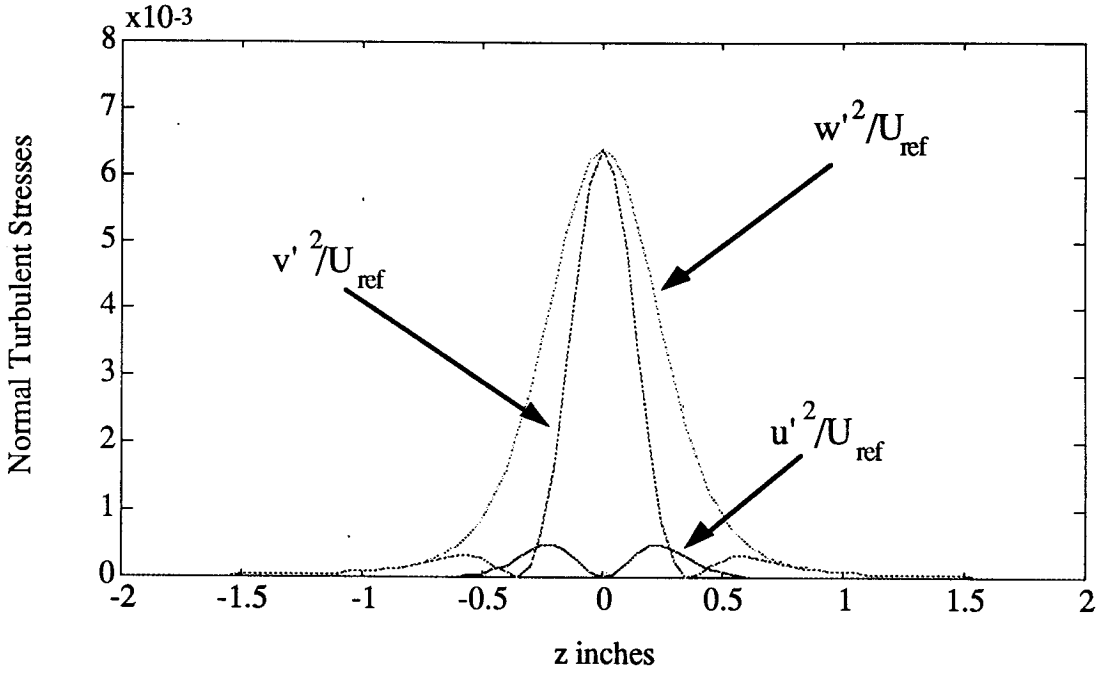

Figure A4: The predicted normal stresses based on the lateral vortex motion model.

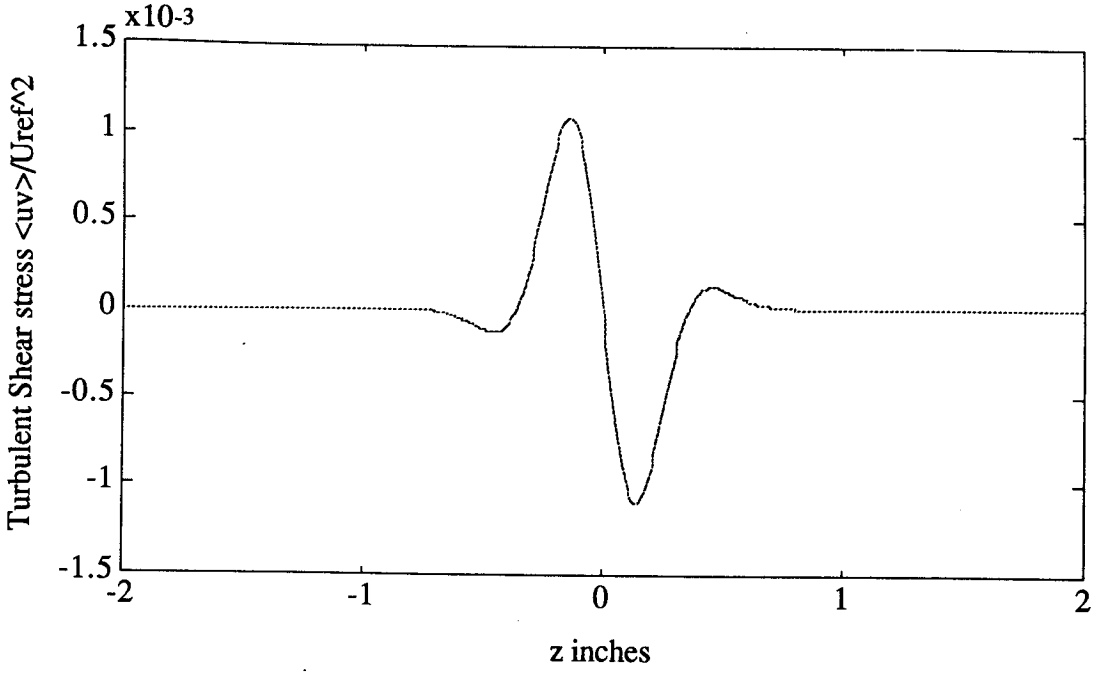

Figure A5; The predicted turbulent shear stress $\langle uv \rangle / U_{ref}^2$.